Journal of Materials Science: Materials in Electronics (2018) 29:9596–9604
https://doi.org/10.1007/s10854-018-8995-2

A comparative study of transport properties of copper doped cadmium selenide thin films at two dopant concentrations

Kriti Sharma[1] · Poonam[2] · G. S. S. Saini[2] · S. K. Tripathi[2]

Received: 17 November 2017 / Accepted: 23 March 2018 / Published online: 10 April 2018
© Springer Science+Business Media, LLC, part of Springer Nature 2018

Abstract

We have explored the effect of Cu dopant concentration on the electrical transport properties of Cu doped CdSe thin films at two concentrations of Cu (at 1 and 5 at.%). Structural, morphological and elemental analysis has been carried out by using X-ray Diffraction (XRD), Scanning electron microscopy (SEM) and Energy Dispersive X-ray analysis (EDX). XRD analysis reveals the hexagonal (wurtzite) structure of nc-CdSe:Cu 1% and nc-CdSe:Cu 5% thin films. EDX analysis determines the atomic weight percentage of Cu in these thin films. SEM studies reveal that the grains are uniformly distributed all over the surface of the substrates for nc-CdSe:Cu 1% and nc-CdSe:Cu 5% thin films. Dark conductivity measurements are made on nc-CdSe:Cu 1% and nc-CdSe:Cu 5% thin films in the temperature range 110–370 K in order to determine the effect of Cu concentration. The obtained results reveal that dark conductivity increases as the Cu dopant concentration increases as compared to undoped nc-CdSe thin films. Dark conductivity graphs show two distinct regions at high and low temperatures with decreasing activation energies. Low temperature data is analyzed using Mott's variable-range hopping model which indicates hopping in localized states near the Fermi level. Various Mott parameters such as the density of localized states $N(E_F)$, characteristic temperature (T_o), hopping distance (R) and hopping energy (W) near the Fermi level are calculated. The concentration of charge carriers and carrier mobility are calculated for nc-CdSe:Cu 1% and nc-CdSe:Cu 5% thin films by using Hall measurements. Constant photocurrent measurement is also performed on Cu 1% and Cu 5% doped CdSe thin films to determine occupied density of states, Urbach parameter and density of defect states. Obtained results show that occupied density of states increases for nc-CdSe:Cu 5% as compared to nc-CdSe:Cu 1% thin films.

1 Introduction

Nanocrystalline semiconductors of II–VI compounds in thin film form hold great promise due to wide range of applications. They possess unique electronic and optical properties which can be easily tuned by varying the sizes and compositions of nanoparticles. Among II–VI compounds, Cadmium Selenide is one of the most promising material which makes it suitable for the development of many interesting applications such as optoelectronic devices [1], solar cells [2], light emitting diodes (LEDs) [3], electroluminescent devices [4] etc. CdSe is an n-type semiconductor material and its band-gap lies in close range with the maximum theoretical range that is attainable for energy conversion efficiency [5]. It has high absorption coefficient in wide spectrum of wavelengths from ultraviolet to infrared regions with a direct band gap of 1.74 eV at 300 K [6]. CdSe mainly exists in three crystalline structures namely hexagonal Wurtzite, cubic Zinc Blende, and Rock Salt structures [7]. Broad range of deposition techniques have been used for the preparation of nanocrystalline CdSe thin films which include vacuum evaporation [8], sputtering [9], chemical bath deposition [10] and spray pyrolysis [11]. The thermal vacuum evaporation is known to be the most suitable technique for the preparation of uniform nc-CdSe thin films owing to easy processability, small deposition time and controllable deposition parameters which allow attainment of desirable properties of the films.

In recent years, various researchers are doping CdSe with transition metals (Fe, Cu, Zn etc.) for practical applications. Doping CdSe with different transition metals find numerous applications in visible region [12]. Deliberate addition of impurity atoms improve the structural, electrical, optical and other characteristic properties of host lattice so that material

✉ S. K. Tripathi
surya@pu.ac.in; surya_tr@yahoo.com

[1] Department of Physics, G.G.D.S.D. College, Sector 32-C, Chandigarh, Panjab, India

[2] Centre of Advanced Study in Physics, Department of Physics, Panjab University, Chandigarh 160014, India

with desired properties can be produced. In recent years, researchers are focusing on copper-doped semiconductor nanocrystals. Several groups have made excellent progress by developing copper-doped nanocrystals as size and composition tunable nanophosphors. These Cu doped CdSe nanocrystals also find applications for LEDs [13], solar concentrators [14] and nanolabels for optical microscopies [15]. Xie et al. [16] have reported the structural and photoelectrical properties of Cu doped CdS thin films prepared by Ultrasonic Spray Pyrolysis and investigated the influence of doping concentration and annealing treatment on these properties. Deng et al. [17] have studied Cu doped CdS thin films and investigated the effect of Cu on microstructure, optical and electrical properties of CdS material. They have also used Cu doped CdS as window layer in CdTe thin film solar cell.

Determination of optical absorption and density of states (DOS) in the sub-gap are important to study the electrical and optical properties of materials and performance of solar cells. A variety of techniques such as photothermal deflection spectroscopy (PDS) [18], Dual Beam Photoconductivity (DBP) [19], electron spin resonance (ESR) [20] and constant photocurrent measurements (CPM) [21] are being used for the determination of absorption coefficient and density of states in the sub-band-gap region. The CPM has a unique advantage as compared to other techniques of being insensitive with surface defects and able to measure both charged and neutral defect densities below the Fermi level [22].

In the present paper, we are reporting the effect of Cu as a dopant on electrical transport properties of CdSe thin films. To compare the effect of Cu as a dopant in CdSe at low and high atomic weight percentages, we have chosen two atomic weight percentages of Cu i.e. 1% and 5% in CdSe. We have also determined sub-band-gap absorption parameters such as sub-band-gap optical absorption coefficient, occupied density of states, density of defects and Urbach energy for Cu 1% and 5% doped CdSe thin films using constant photocurrent method (CPM). The determination of sub-band-gap absorption, density of defects and Urbach energy is crucial in developing electronic and photovoltaic devices.

2 Experimental

The starting material i.e. Cu (1%)-doped $Cd_{35}Se_{65}$ and Cu (5%)-doped $Cd_{35}Se_{65}$ is prepared by the melt-quench technique [23] and then used as a source to prepare thin films. Constituent elements (5 N pure) are weighed according to their atomic percentages and sealed in quartz ampoules in vacuum 2×10^{-5} mbar. The sealed ampoules are kept inside the furnace where the temperature is increased up to 1000 °C at a heating rate of 2–3°C/min. The ampoules are frequently rocked for 24 h at the highest temperature of the constituent elements to make the melt homogeneous. The quenching is done in liquid N_2. nc-CdSe:Cu 1% and nc-CdSe:Cu 5% thin films are prepared by physical vapor deposition using the Inert Gas Condensation technique in the presence of argon as inert gas at room temperature and base pressure of 2×10^{-5} mbar on well-degassed Corning 7059 glass substrates. The films are kept in deposition chamber in dark for 24 h before taking optical measurements to attain thermodynamic equilibrium. The thickness of the nc-CdSe:Cu 1% and nc-CdSe:Cu 5% thin films is measured by the weight difference method using a sensitive microbalance. Crystallographic study is carried out on the nc-CdSe:Cu 1% and nc-CdSe:Cu 5% thin films using a Spinner 3064 XPERT-PRO X-ray diffractometer using CuKα radiation in the 2θ range from 10° to 80°. The accelerating voltage is set at 45 kV with a current of 40 mA. The microstructure of the nc-CdSe:Cu 1% and nc-CdSe:Cu 5% thin films on the glass substrate has been studied by using a Jeol Scanning Electron Microscope (JSM-6610 LV). EDX analysis is carried out by energy dispersive spectrometer (EDS) coupled with JSM-6610 LV. The electrical measurements of these thin films are carried out in a specially designed metallic sample holder where heat filtered white light of the intensity 200 W tungsten lamp is shone through a transparent quartz window. A vacuum of 2×10^{-3} mbar is maintained throughout these measurements. Light intensity is measured using a digital luxmeter (MASTECH, MS6610). Planar geometry of the films (length ~ 1.2 cm; electrode gap ~ 8×10^{-2} cm) is used for the electrical measurements. Thick Indium (In) electrodes used for electrical contacts are deposited by thermal evaporation at room temperature. For Hall measurements, four Indium electrodes are formed on the surface of nc-CdSe:Cu 1% and nc-CdSe:Cu 5% thin films. Typical sample dimensions are ~ 2.5×2.5 cm^2 and width of electrodes ~ 1 mm^2. The photocurrent (I_{ph}) is obtained after subtracting the dark current (I_d) from the current measured in the presence of light. The dark and photocurrent are noted using a Keithley Electrometer (6517A). CPM measurements are carried out using planar Indium electrodes with a separation of 0.8 mm. A bias of 100 V is used for the measurement of photocurrent. Halogen lamp is used as light source. The focused light from the light source is allowed to pass through chopper (AMETEK Model 197) chopped at 200 Hz, monochromator and beam splitter. The intensity of the incoming beam is monitored using a calibrated Si photodiode. The variation in the intensity of light is achieved by changing the power to the halogen lamp. The photocurrent is kept constant by varying the lamp supply voltage. The constant value of the photocurrent is read across a 1 MΩ resistor using a lock-in amplifier [EG&G Model 7265].

3 Result and discussion

The thickness of nc-CdSe:Cu 1% and nc-CdSe:Cu 5% thin films is determined gravimetrically by measuring the change in the weight of the substrate before and after the film deposition and using the bulk density of the material used. The thickness of nc-CdSe:Cu 1% and nc-CdSe:Cu 5% thin films is calculated to be approximately 170 nm. The XRD pattern of nc-CdSe:Cu 1% and nc-CdSe:Cu 5% thin films is shown in Fig. 1. The observation of intense diffraction peaks at $2\theta = 23.4°$ and $2\theta = 25.2°$ for nc-CdSe:Cu 1% correspond to (100) and (002) planes of hexagonal (wurtzite) structure of CdSe. Additional two small intensity peaks at $2\theta = 29.7°$ and $2\theta = 41.1°$ reveal the existence of (103) and (106) planes of hexagonal structure corresponding to Copper Selenide. The appearance of (103) and (106) planes corresponding to Copper Selenide after doping with Cu 1% in CdSe suggests that Cu^{2+} ions replace the Cd^{2+} ions and incorporate in the CdSe lattice. As the Cu concentration increases to 5%, the intensity of the peak corresponding to (100) and (002) planes decrease and (103) plane increases sharply which suggests that the growth of nanoparticles along (103) plane in Cu 5% doped CdSe thin films. The average grain size has been calculated by the Debye–Scherrer relationship and is found to be D = 31 and 44 nm for CdSe:Cu (1%) and CdSe:Cu (5%), respectively. The average grain size for undoped nc-CdSe thin films is 12 nm [24]. Thus, the grain size increases as Cu dopant concentration increases.

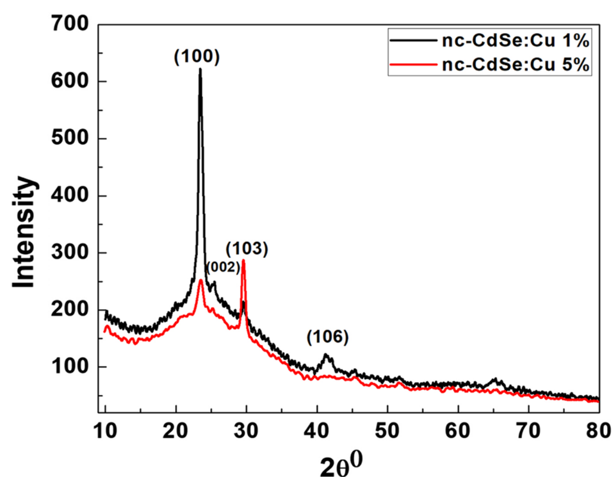

Fig. 1 XRD pattern of nc-CdSe:Cu 1% and nc-CdSe:Cu 5% thin films

Figure 2a, b shows the surface morphology of nc-CdSe:Cu 1% and nc-CdSe:Cu 5% thin films using SEM. From the micrographs, it is observed that films are homogenous, without cracks or holes and that they cover the glass substrate well. It is also observed from the figure that the grain size increases as the doping concentration of Cu increases. Energy dispersive X-ray spectroscopy (EDX) spectra of nc-CdSe:Cu 1% and nc-CdSe:Cu 5% thin films is shown in Fig. 3a, b. The elemental analysis is carried out only for Cd, Se and Cu. The relative atomic percentage is Cu:Se:Cd ~ 1.28:61.58:37.14 for nc-CdSe:Cu 1% thin films and Cu:Se:Cd ~ 5.1:59.37:35.52 for nc-CdSe:Cu 5% thin films.

The temperature dependence of the DC conductivity (σ_d) of nc-CdSe:Cu 1% and nc-CdSe:Cu 5% thin films has been studied and ln σ_d vs. 1000/T curves are plotted in Fig. 4. It has been observed that the conductivity of the both the samples increase with increase in temperature which indicates the semiconductor behavior of the films. ln σ_d vs. 1000/T curve for undoped nc-CdSe thin film [25] has been shown in the inset of Fig. 4 for comparison. On the basis of nature

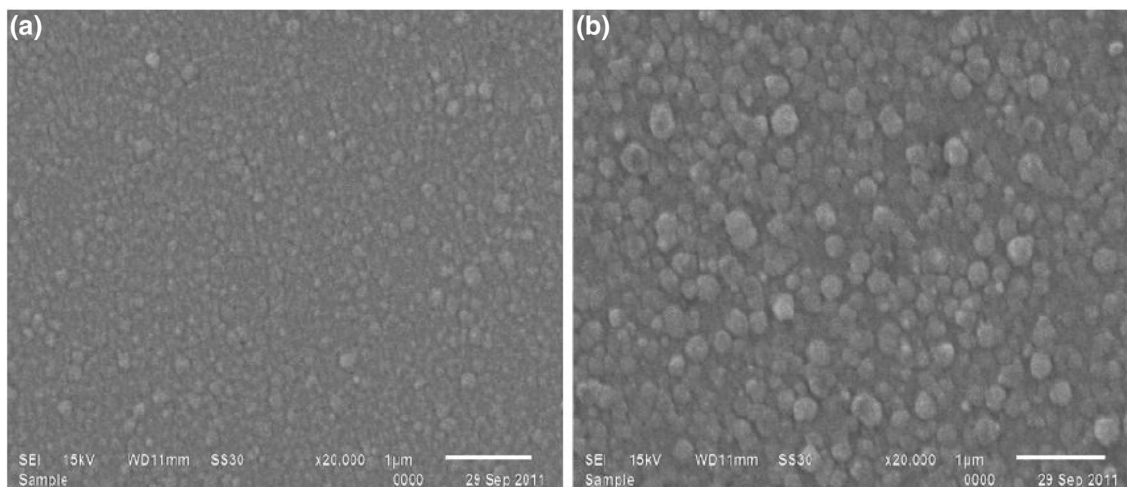

Fig. 2 SEM image of **a** nc-CdSe:Cu 1% thin film, **b** nc-Cd-CdSe:Cu 5% thin film

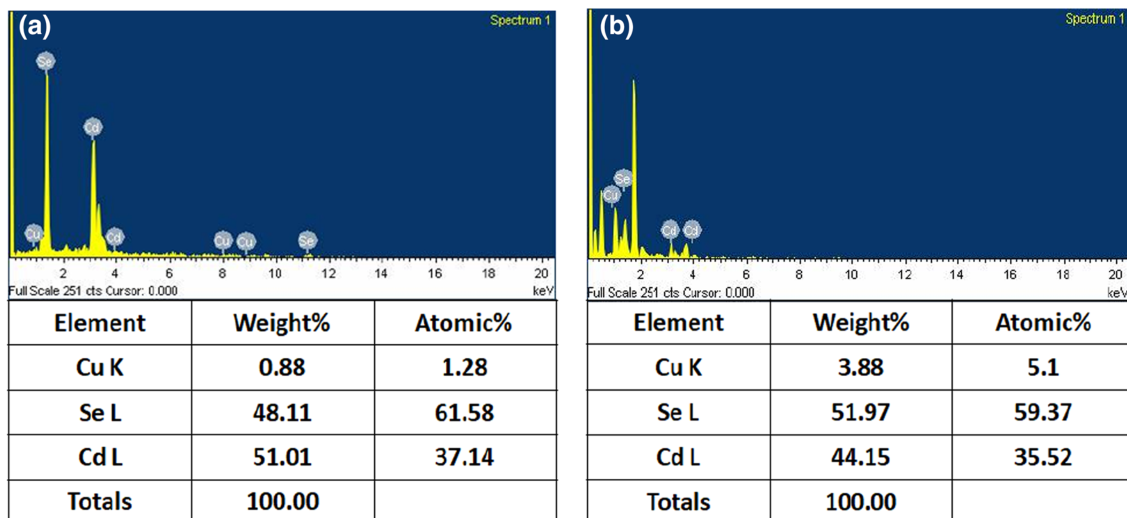

(a)

Element	Weight%	Atomic%
Cu K	0.88	1.28
Se L	48.11	61.58
Cd L	51.01	37.14
Totals	100.00	

(b)

Element	Weight%	Atomic%
Cu K	3.88	5.1
Se L	51.97	59.37
Cd L	44.15	35.52
Totals	100.00	

Fig. 3 EDX pattern of **a** nc-CdSe:Cu 1%, **b** nc-CdSe:Cu 5% thin films

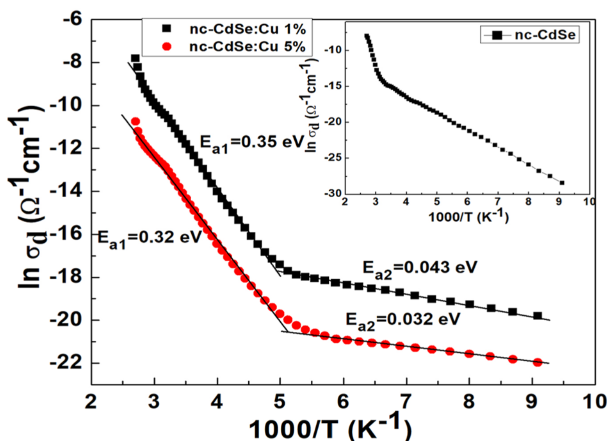

Fig. 4 The plot of ln σ_d vs. 1000/T for nc-CdSe:Cu 1% and nc-CdSe:Cu 5% thin films. Inset shows the plot of ln σ_d vs. 1000/T for undoped nc-CdSe thin film

of slope, the whole temperature range (100–370 K) can be divided in two regions: high temperature region (165–370 K) and low temperature region (100–160 K) which contribute to two conduction mechanisms. The variation of conductivity with temperature can be expressed as:

$$\sigma = \sigma_1 \exp\left(\frac{-E_{a1}}{kT}\right) + \sigma_2 \exp\left(\frac{-E_{a2}}{kT}\right) \tag{1}$$

where σ_1 and σ_2 represent the pre-exponential factors, E_{a1} and E_{a2} are the activation energies, k is the Boltzmann constant and T is the temperature. The first term in Eq. (1) corresponds to the conduction in extended states and the second term corresponds to the conduction in localized states which takes place as a result of hopping of charge carriers from one impurity level to an adjacent one. At low temperature, conduction is due to thermally assisted tunneling of charge carriers in the localized states in the band tails and the carriers move from one impurity level to another with the help of phonons [26]. The values of σ_d at room temperature (300 K) for undoped nc-CdSe [25] and Cu 1% and 5% doped nc-CdSe are mentioned in Table 1. The value of σ_d increases after doping with Cu 1% and further increases for Cu 5% doped CdSe thin films as compared to undoped nc-CdSe thin films. As the Cu doping concentration increases, the value of σ_d increases as compared to undoped nc-CdSe which may be due to substitution of Cu^{2+} ions at the sites of Cd^{2+} and improvement in grain size as confirmed from XRD analysis, thus reducing the grain boundary scattering.

The low temperature experimental data of the temperature dependence of σ_d in the temperature range 100–160 K has been analyzed using Mott's variable-range hopping (VRH) model. The conductivity in the low-temperature region increases slowly with increase in temperature, which

Table 1 Electrical parameters of nc-CdSe, nc-CdSe:Cu 1% and nc-CdSe:Cu 5% thin films

Sample	σ_d at 300 K (Ω^{-1} cm^{-1})	T_o (K)	$N(E_f)$ (eV^{-1} cm^{-3})	R (cm)	W (eV)	αR
nc-CdSe [25]	4.13×10^{-7}	4.23×10^{9}	4.98×10^{16}	2.78×10^{-6}	0.18	3447.2
nc-CdSe:Cu 1%	1.32×10^{-6}	2.73×10^{6}	7.69×10^{19}	4.43×10^{-7}	0.029	549.3
nc-CdSe:Cu 5%	1.55×10^{-5}	6.38×10^{6}	3.29×10^{19}	5.61×10^{-7}	0.035	695.6

suggests that the conduction is due to the VRH in the localized states near the Fermi level [27]. The VRH conduction occurs at temperatures at which the phonons do not have sufficient energy to transfer to a nearest neighbor atom and the charge carrier hops from a neutral atom to another neutral atom situated at the same energy level which can be positioned many interatomic distances away [28]. This VRH mechanism is characterized by Mott's [29] expression:

$$\sigma_d T^{1/2} = \sigma_O \exp\left[-\left(\frac{T_O}{T}\right)^{1/4}\right] \tag{2}$$

here σ_0 is the pre-exponential factor which depends on frequencies and the characteristic Mott temperature T_o is related to the density of states $N(E_F)$ at the Fermi level and the inverse-fall-off length of the wave function of a localized state near the Fermi-Level α by the following relation [30]:

$$T_O = C_O \frac{\alpha^3}{kN(E_F)} \tag{3}$$

where $N(E_F)$ is the density of states at the Fermi level and $C_o = 18$ is a numerical constant which depends on the detailed assumptions. α is the coefficient of the exponential decay of the localized states wave function and is assumed to be 0.124 $\mathring{A}^{-1}$ [31–33]. Figure 5 shows the plot of ln $\sigma T^{1/2}$ vs. $T^{-1/4}$ for nc-CdSe:Cu 1% and nc-CdSe:Cu 5% thin films. According to Mott [28], the linear region of this plot represents electron transport by hopping among localized states. Thus the experimental data obey Mott's VRH relation [34], giving rise to a linear relationship between ln ($\sigma T^{1/2}$) and ($T^{-1/4}$) as is clear from Fig. 5. Therefore, the conduction mechanism at low temperature is due to the hopping of the charge carriers among the localized states. Other Mott parameters, the hopping distance R and average energy W are determined at T = 140 K using the following relations [35]:

$$R = \left[\frac{9}{8\pi\alpha kTN(E_F)}\right]^{\frac{1}{4}} \tag{4}$$

$$W = 0.2k\left(T_O T^3\right)^{1/4} \tag{5}$$

From the slope of Fig. 5, we have calculated various Mott parameters such as the characteristic Mott temperature (T_o), density of states [$N(E_F)$] at the Fermi level, hopping distance (R) and hopping energy (W) are calculated for nc-CdSe:Cu 1% and nc-CdSe:Cu 5% thin films at 140 K as listed in Table 1. It is evident from the table that density of states near Fermi level increases after Cu doping at 1 and 5% as compared to undoped nc-CdSe thin films.

According to Mott and Davis [36, 37], αR and W should have values greater than unity and kT respectively, for VRH conduction. It is evident from this Table 2 $\alpha R > 1$ and $W > kT$, which shows a close agreement with Mott's VRH [38, 39]. Degree of localization of the carriers in the trap states, indicated by $\alpha R > 1$, shows that the charges are highly localized.

Carrier concentration and the nature of charge carriers at room temperature (300 K) have been determined using Hall measurements from the slope of current (I) vs. Hall voltage (V_H) as shown in Fig. 6 for nc-CdSe:Cu 1% and nc-CdSe:Cu 5% thin films respectively. The values of carrier mobility (μ_H) and carrier concentration (n) for nc-CdSe [25], nc-CdSe:Cu 1% and nc-CdSe:Cu 5% thin films are given in Table 2. The value of carrier concentration increases for nc-CdSe:Cu 5% thin films as compared to undoped nc-CdSe and nc-CdSe:Cu 1% thin films which are almost comparable. At higher doping concentrations of Cu i.e. at 5%, an increase in grain size has been observed from XRD, which ultimately reduces grain boundary scattering resulting in an increase in carrier concentration. From the results of Hall measurements we have observed negative sign of Hall voltage for nc-CdSe [25] and nc-CdSe:Cu 1% thin films but positive sign of Hall voltage for nc-CdSe:Cu 5% thin films. Thus the nature of charge carriers changes from n-type to p-type as the doping

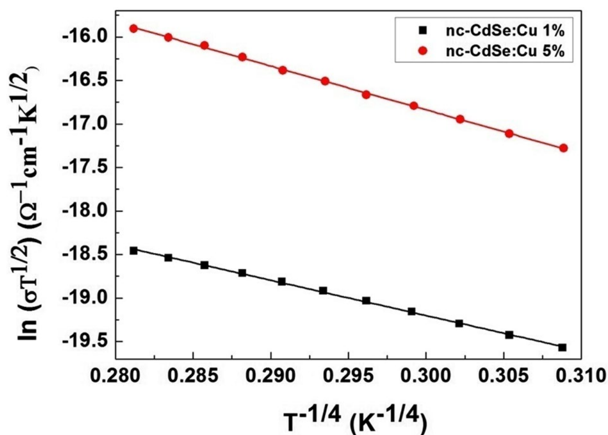

Fig. 5 The plot of ln $\sigma T^{1/2}$ vs. $T^{-1/4}$ for nc-CdSe:Cu 1% and nc-CdSe:Cu 5% thin films

Table 2 Parameters calculated from Hall measurements for nc-CdSe, nc-CdSe:Cu 1% and nc-CdSe:Cu 5% thin films

Sample	Carrier mobility μ (cm^2/V s)	Carrier Concentration n (cm^{-3})
nc-CdSe [25]	21.42	1.20×10^{11}
nc-CdSe:Cu 1%	70.53	1.10×10^{11}
nc-CdSe:Cu 5%	55.35	1.75×10^{12}

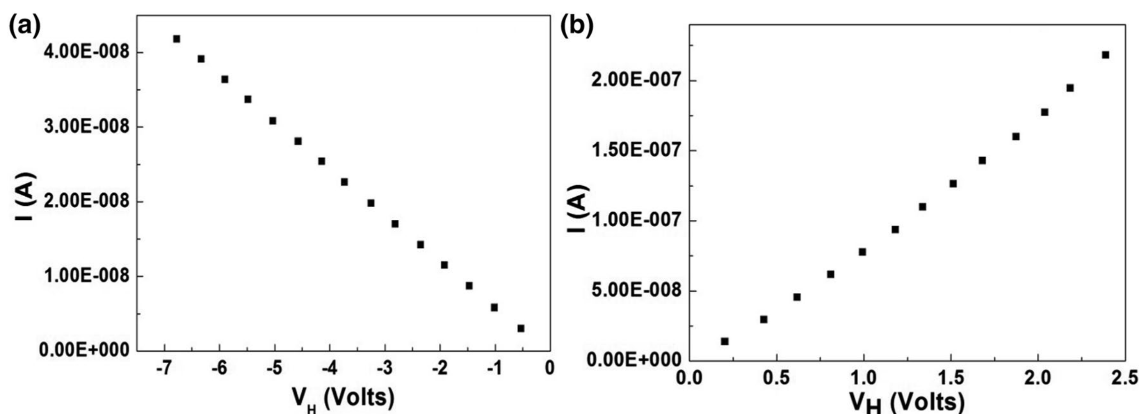

Fig. 6 The plot of Hall voltage (V_H) vs. current for **a** nc-CdSe:Cu 1% and **b** nc-CdSe:Cu 5% thin film

concentration of Cu is increased to 5%. At high concentration of Cu dopant (at 5%) there is an enhanced substitution of Cd^{2+} by Cu^{2+} which is confirmed by XRD analysis in which the intensity of peak (103) corresponding to hexagonal plane of Copper Selenide increases sharply as compared to Cu doping at 1%. Since Copper Selenide is p-type, thus the nature of charge carriers changes from n-type to p-type as the Cu concentration increases from 1 to 5%.

The main idea of using constant photocurrent (CPM) Method is that the light intensity is adjusted so that the value of measured photocurrent remains constant as the energy of exciting photons is changed, the energy dependence of optical absorption coefficient can be deduced [40].

In CPM the photocurrent is excited in the sample by using low intensity monochromatic beam. Electric field is applied to coplanar ohmic electrodes which is used to measure resultant photocurrent generated by probe beam. For thin films and in the sub-band-gap part of absorption spectrum ($\alpha d \ll 1$) the photocurrent is proportional to [41]:

$$I\alpha N(1 - R)\alpha\eta\tau h\mu_p F \quad (6)$$

where N is the number of incident photons, R is the reflectivity, η is the quantum yield (the chance that the absorbed photons will create free carriers), τ is the lifetime of the carrier, h is the hole charge, μ_p is the hole mobility and F is the applied field. R is assumed to be independent of photon energy in the region of experimental interest.

In CPM if the measured photocurrent is kept constant over the whole spectral range by adjusting the photon flux N(hν) both the mobility μ and lifetime τ are expected to remain constant when the temperature does not vary [42]. So above equation can be written as:

$$\alpha(h\nu) = \frac{\text{constant}}{N} \quad (7)$$

Thus by measuring the number of photons that keep the photocurrent constant the spectral dependence of optical absorption coefficient in the sub-band-gap region can be determined. The total number of photons have been calculated from the formula [43]:

$$N = \frac{10^{15}P(h\nu)}{1.6E(h\nu)}\,cm^{-2}\,s^{-1} \quad (8)$$

where P(hν) ($mWcm^{-2}$) is the power of incident illumination at energy E(hν) (eV). The experimental variation of N vs. E(hν) is first recorded, which is then plotted as 1/N vs. E(hν). A normalization is then carried out according to (1/N)/(1/N_{max}). In the weak absorption region, the absorption coefficient α is obtained by multiplying the inverse of number of photons by the inverse of the thickness 1/d up to the peak position [44] and is written as:

$$\alpha = \frac{1/n_{ph}}{1/n_{phmax}}\frac{1}{d} \quad (9)$$

The value of α so obtained is then matched with absorption coefficient α at any chosen point, obtained from reflection and transmission measurements in the visible region, and thus a final curve of the absorption coefficient α is obtained at different energy values. Figure 7 shows the dependence of α on photon energy of nc-CdSe:Cu 1% and nc-CdSe:Cu 5% thin films using CPM. It is observed from the figure that sub-band-gap optical absorption coefficient increases for nc-CdSe:Cu 1% thin films as compared to undoped nc-CdSe and further increases for nc-CdSe:Cu 5% thin films. The values of subband gap optical absorption coefficient deduced from CPM measurements (α_{CPM}) at 1.48 eV for nc-CdSe (shown for comparison purpose [21]), nc-CdSe:Cu 1% and nc-CdSe:Cu 5% thin films are mentioned in Table 3. It is clear from the table that sub-band-gap optical absorption coefficient increases as the Cu doping concentration increases.

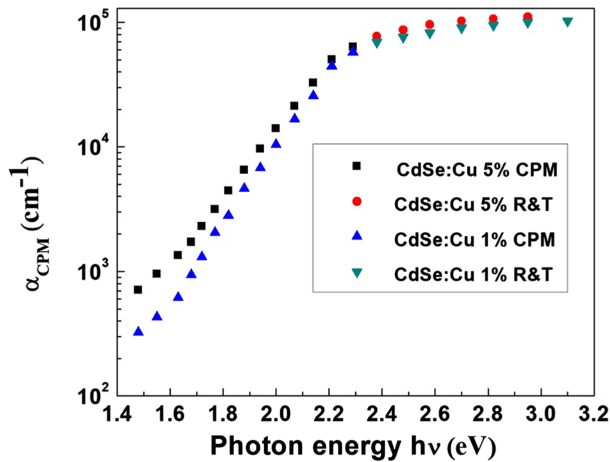

Fig. 7 Energy dependence of α_{CPM} of nc-CdSe:Cu 1% and nc-CdSe:Cu 5% thin films

Table 3 The values of subband gap optical absorption coefficient (α_{CPM}) at 1.48 eV, Urbach energy (E_U), concentration of surface defects (N_t) for nc-CdSe, nc-CdSe:Cu 1% and nc-CdSe:Cu 5% thin films

	α_{CPM} (cm^{-1})	E_U (eV)	N_t (cm^{-3})
nc-CdSe [21]	27.59	0.12	8.21×10^{19}
nc-CdSe:Cu 1%	323.58	0.14	2.40×10^{20}
nc-CdSe:Cu 5%	443	0.22	4.03×10^{20}

The α(hν) curve (as seen from Fig. 7) consists of mainly three regions [42, 45]. The saturation region at higher energies is due to direct valence band to conduction band transition. Second region is an exponential Urbach edge region where absorption coefficient α varies as $\alpha = \alpha_o \exp\left(\frac{h\nu}{E_U}\right)$. The exponential portion is referred to as Urbach tail and E_U is the characteristic energy of Urbach tail which is representative of disorder. This region is due to transitions between localized states in valence band tail & extended and localized states in the conduction band and conduction band tail respectively. Third region which is defect absorption region is due to photon absorption by gap states. This region is essentially determined by the optical transitions involving the deep localized defect states. The Urbach parameter (E_U) which is characteristic of disorder in the sample is estimated for nc-CdSe:Cu 1% and nc-CdSe:Cu 5% thin films. The values are mentioned in Table 3. The value of E_U for undoped nc-CdSe is also mentioned in table for comparison [21]. It is clear from the values that the structural disorder increases as the Cu dopant concentration increases.

The absorption coefficient α can be written as the convolution integral of initial $N_i(E)$ and final $N_f(E+h\nu)$ states that are involved in electronic transitions. The optical absorption coefficient α(hν) can be written [46] as:

$$\alpha(h\nu) = \frac{A}{h\nu}\int_{-\infty}^{\infty} N_i(E)f(E)\{1 - f(E + h\nu)\}N_f(E + h\nu)dE \tag{10}$$

where A is a constant containing the optical matrix element, $N_i(E)$ and $N_f(E+h\nu)$ are the initial and final electronic states, hν is the photon energy and f(E) is the Fermi–Dirac distribution. Since CPM detects only the electronic transitions from occupied states to the conduction band [40]. Thus a simple method was proposed by Hata and Wagner [47] based on deconvolution of the occupied DOS from CPM spectra. In the CPM technique, the deep empty states below the conduction edge need not be considered. Thus, the conduction band $N_f(E+h\nu)/h\nu$ can be approximated with a step function $N_c\theta(E+h\nu-E_c)$, where N_c is the DOS at the conduction edge E_c and $\theta(E+h\nu-E_c)$ is the Heaviside function $\theta=1$ for $E \geq Ec - h\nu$, $\theta=0$ for $E < E_c - h\nu$. So, Eq. (10) becomes:

$$\alpha_{CPM}(h\nu) \cong AN_C \int_{-\infty}^{\infty} N_i(E)f(E)\theta(E + h\nu - E_C)dE \tag{11}$$

where E_c is the conduction edge. From Eq. (11) we obtain:

$$N_i(E)f(E) = \frac{1}{AN_C}\left\{\frac{d\alpha(h\nu)}{d(h\nu)}\right\}_{h\nu=E_C-E} \tag{12}$$

we deduce that the occupied states as a first approximation result to be the derivative of the CPM spectrum with respect to photon energy. Occupied gap state density of states is plotted in Fig. 8 for nc-CdSe:Cu 1% and nc-CdSe:Cu 5% thin films. From this graph, we deduce that occupied density of states increases for Cu 5% doped CdSe thin films as compared to Cu 1% doped CdSe thin films.

Considering the lowest energy part of the Urbach tail where the deep defect absorption dominates we make a quantitative estimation of the concentration of the defects. It is assumed that the concentration of the surface defect states (N_t), at the starting point of the deviation from the high-energy exponential part of the Urbach tail, is of the same order as that of the tail states (N_u). The distribution of the defect states in the valence band tail [29] is estimated by following relation:

$$N_t \approx N_u \approx N_v \exp\left\{-(E - E_v)/E_u\right\} \tag{13}$$

Accepting $N_v \approx 10^{21}$ cm^{-3} [48] for the density of states at the top of the valence band E_v, E_u for the slope of the Urbach tail absorption and $(E-E_v) \approx 0.2$–0.3 eV, concentration of defect states is estimated. The values of defect states for undoped nc-CdSe is 8.21×10^{19} cm^{-3} [21], for nc-CdSe:Cu 1% is 2.40×10^{20} cm^{-3} and for nc-CdSe:Cu 5% thin films is 4.03×10^{20} cm^{-3}. These values are also mentioned

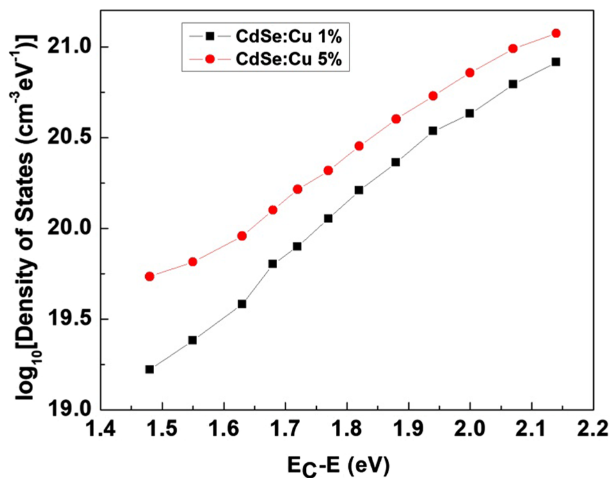

Fig. 8 Occupied density of states of nc-CdSe:Cu 1% and nc-CdSe:Cu 5% thin films

in Table 3. Thus the concentration of surface defect states increases as the Cu doping concentration increases.

4 Conclusion

Thus in the present work, we have made an effort to study charge carrier transport properties of Cu doped CdSe thin films which are potential candidates for solar cells and other optoelectronic devices. XRD data reveals the hexagonal structure of nc-CdSe:Cu 1% and nc-CdSe:Cu 5% thin films. SEM investigation reveals that the grain size increases for nc-CdSe:Cu 5% thin film as compared to nc-CdSe:Cu 1% thin films. EDX data confirms the atomic weight percentage of Cu in nc-CdSe:Cu 1% and nc-CdSe:Cu 5% thin films. We have observed that dark conductivity increases as the Cu doping concentration increases. Density of states near Fermi level increases with increase in Cu doping concentration as calculated from Mott VRH Model. Results of Hall measurements reveal that carrier concentration increases for Cu 5% doped CdSe thin films as compared to undoped and Cu 1% doped CdSe thin films. Cu 1% doped CdSe thin films are n-type while in case of nc-CdSe:Cu 5% the charge carriers change sign and these are of p-type. Sub-band-gap optical absorption coefficient, Urbach parameter and occupied density of states are estimated from CPM for nc-CdSe:Cu 1% and nc-CdSe:Cu 5% thin films. These are found to increase as the Cu doping concentration increases.

References

1. M.Z. Hu, T. Zhu, Nanoscale Res. Lett. **10**, 469 (2015)
2. F. Huang, L. Zhang, Q. Zhang, J. Hou, H. Wang, H. Wang, S. Peng, J. Liu, G. Cao, ACS Appl. Mater. Interfaces **8**, 34482 (2016)
3. M.-L. Tu, Y.-K. Su, R.-T. Chen, Nanoscale Res. Lett. **9**, 611 (2014)
4. B.H. Kang, J.S. Lee, S.W. Lee, S.W. Kim, J.W. Lee, S.A. Gopalan, J.S. Park, D.H. Kwon, J.H. Bae, H.R. Kim, S.W. Kang, Sci. Rep. **6**, 34659 (2016)
5. K.B. Chaudhari, N.M. Gosavi, N.G. Deshpande, S.R. Gosavi, J. Sci.: Adv. Mater. Dev. **1**, 476 (2016)
6. S.J. Lim, A. Schleife, A.M. Smith, Nat. Commun. **8**, 14849 (2017)
7. J. Zhao, Y. Zeng, Q. Yang, Y. Li, L. Cui, C. Liu, J. Cryst. Growth **329**, 1 (2011)
8. V. Kumar, D.K. Sharma, K. Sharma, D.K. Dwivedi, Appl. Phys. A **122**, 960 (2016)
9. M.K. Khalaf, B.A.M. ALhilli, A.I. Khudiar, A.Abd Alzahra, Photon. Nanostruct. Fund. Appl. **18**, 59 (2016)
10. Y. Choi, M. Seol, W. Kim, K. Yong, J. Phys. Chem. C **118**, 5664 (2014)
11. T. Logu, K. Sankarasubramanian, P. Soundarrajan, K. Sethuraman, Electron. Mater. Lett. **11**, 206 (2015)
12. B.F.P. McVey, J. Butkus, J.E. Halpert, J.M. Hodgkiss, R.D. Tilley, J. Phys. Chem. Lett. **6**, 1573 (2015)
13. X. Wang, X. Yan, W. Li, K. Sun, Adv. Mater. **24**, 2742 (2012)
14. L.R. Bradshaw, K.E. Knowles, S. McDowall, D.R. Gamelin, Nano Lett. **15**, 1315 (2015)
15. S.M. Ng, M. Koneswaranb, R. Narayanaswamy, RSC Adv. **6**, 21624 (2016)
16. R. Xie, J. Su, M. Li, L. Guo, Int. J. Photoenergy **2013**, 1 (2013)
17. Y. Deng, J. Yang, R. Yang, K. Shen, D. Wang, D. Wang, AIP Adv. **6**, 015203 (2016)
18. A.R. Krause, C.V. Neste, L. Senesac, T. Thundat, E. Finot, J. Appl. Phys. **103**, 094906 (2008)
19. M. Gunes, H. Hamza Cansever, G. Yilmaz, V. Smirnov, F. Finger, R. Bruggemann, J. Non-Cryst. Solids **358**, 2074 (2012)
20. K.M. Krishna, H. Ebisu, K. Hagimoto, Y. Hayashi, T. Soga, T. Jimbo, M. Umeno, Appl. Phys. Lett. **78**, 294 (2001)
21. K. Sharma, A.S. Al-Kabbi, G.S.S. Saini, S.K. Tripathi, Curr. Appl. Phys. **13**, 964 (2013)
22. R.H. Bube, M.N. L.E.Benatar, D. Grimbergen, Redfield, J. Appl. Phys. **72**, 5766 (1992)
23. K. Sharma, A.S. Al-Kabbi, G.S.S. Saini, S.K. Tripathi, J. Alloys Compd. **651**, 42 (2015)
24. K. Sharma, A.S. Al-Kabbi, G.S.S. Saini, S.K. Tripathi, Mater. Res. Bull. **47**, 1400 (2012)
25. K. Sharma, A.S. Al-Kabbi, G.S.S. Saini, S.K. Tripathi, J. Alloys Compd. **564**, 42 (2013)
26. K. Asadi, A.J. Kronemeijer, T. Cramer, L.J. Anton Koster, W.M.P. Blom, Dago M. de Leeuw, Nat. Commun. **4**, 1710 (2013)
27. K. Sharma, A.S. Al-Kabbi, G.S.S. Saini, S.K. Tripathi, Appl. Phys. A **108**, 911 (2012)
28. N.F. Mott, Philos. Mag. **19**, 835 (1969)
29. N.F. Mott, J. Non-Cryst. Solids **8**, 191 (1972)
30. N.F. Mott, E.A. Davis, *Electronic Processes in Non-Crystalline Materials*, 2nd edn. (Clarendon, Oxford, 1979)
31. S. Ramchandar Rao, M. Nagabhooshanam, V.Hari Babu, Cryst. Res. Technol. **25**, 55 (2006)
32. M. Thamilselvan, K. Premnazeer, D. Mangalaraj, Sa.K. Narayandass, J. Yi, Cryst. Res. Technol. **39**, 137 (2004)
33. C.H. Seager, G.E. Pike, Phys. Rev. B **10**, 1435 (1974)
34. A.F. Qasrawi, M.M. Shukri Ahmed, Cryst. Res. Technol. **41**, 364 (2006)
35. N.F. Mott, E.A. Davis, *Electronic Processes in Non-crystalline Materials* (Clarendon, Oxford, 1970)
36. T.G. Abdel-Malik, R.M. Abdel-Latif, A. Sawaby, S.M. Ahmed, J. Appl. Sci. Res. **4**, 331 (2008)
37. N.F. Mott, E.A. Davis, Philos. Mag. **22**, 903 (1970)

38. M.G. Syed Ahamed Basheer, K.S. Rajni, V.S. Vidhya, V. Swaminathan, A. Thayumanavan, K.R. Murali, M. Jayachandran, Cryst. Res. Technol. **46**, 261 (2011)
39. A.A. Yadav, E.U. Masumdar, Mater. Res. Bull. **45**, 1455 (2010)
40. J. Kocka, M. Vanecek, A. Triska, *Amorphous Silicon and Related Materials* (World Scientific, Singapore, 1988). p. 297
41. J. Willekens, M. Brinza, T. Aernouts, J. Poortmans, G.J. Adriaenssens, J. Non-Cryst. Solids **352**, 1675 (2006)
42. P. Sládek, P. Sťahel, P.R.I. Cabarrocas, P. Morin, Philos. Mag. B **77**, 1049 (1998)
43. A. Madan, M.P. Shaw, *Physics and Applications of Amorphous Semiconductors* (Academic Press, New York, 1988), p. 161
44. M. Vanecek, J. Kocka, J. Stuchlik, A. Triska, Solid State Commun. **39**, 1199 (1981)
45. A. Tyagi, O.S. Panwar, B.S. Satyanarayan, P.N. Dixit, T. Seth, R. Bhattacharyya, V.V. Shah, Thin Solid Films **203**, 251 (1991)
46. M. Vanecek, A. Abraham, O. Stika, J. Stuchlik, J. Kocka, Phys. Stat. Sol. A **83**, 617 (1984)
47. H. Hata, S. Wagner, *Amorphous Silicon Technology*. (Materials Research Society, Pittsburg, 1991). p. 611
48. F. Wang, T. Fischer, T. Muschik, R. Schwarz, Philos. Mag. B **68**, 737 (1993)